FOR FURTHER TRAN

AD A055773

PANA-AIR-2

ATMOSPHERIC DENSITY MEASUREMENT IN THE MIDDLE ATMOSPHERE

Bach Sellers
Jean L. Hunerwadel

Panametrics, Inc.
221 Crescent Street
Waltham, Massachusetts 02154

DDC FILE COPY

August, 1977

Annual Report

GEOSCIENCES DIVISION
ARMY RESEARCH OFFICE
RESEARCH TRIANGLE PARK, NC 27709

DDC
RECEIVED
JUN 29 1978
A

DISTRIBUTION STATEMENT A
Approved for public release;
Distribution Unlimited

78 06 29 056

Unclassified

SECURITY CLASSIFICATION OF THIS PAGE (When Data Entered)

REPORT DOCUMENTATION PAGE	READ INSTRUCTIONS BEFORE COMPLETING FORM
1. REPORT NUMBER: PANA-AIR-2	2. GOVT ACCESSION NO. / 3. RECIPIENT'S CATALOG NUMBER
4. TITLE (and Subtitle): Atmospheric Density Measurement in the Middle Atmosphere	5. TYPE OF REPORT & PERIOD COVERED: Annual Rept. 1 May 1976 - 30 June 1977
	6. PERFORMING ORG. REPORT NUMBER
7. AUTHOR(s): Bach Sellers, Jean L. Hunerwadel	8. CONTRACT OR GRANT NUMBER(s): DAAG29-76-C-0041
9. PERFORMING ORGANIZATION NAME AND ADDRESS: Panametrics, Inc. 221 Crescent St. Waltham MA 02154	10. PROGRAM ELEMENT, PROJECT, TASK AREA & WORK UNIT NUMBERS
11. CONTROLLING OFFICE NAME AND ADDRESS: Geosciences Division, Army Research Office, Research Triangle Park, NC 27709	12. REPORT DATE: August 1977; 13. NUMBER OF PAGES: 41
14. MONITORING AGENCY NAME & ADDRESS(if different from Controlling Office) 42p.	15. SECURITY CLASS. (of this report): Unclassified; 15a. DECLASSIFICATION/DOWNGRADING SCHEDULE

16. DISTRIBUTION STATEMENT (of this Report)

Approved for public release, distribution unlimited. Reproduction in whole or in part is permitted for any purpose of the United States Government.

17. DISTRIBUTION STATEMENT (of the abstract entered in Block 20, if different from Report)

18. SUPPLEMENTARY NOTES

19. KEY WORDS (Continue on reverse side if necessary and identify by block number)

Atmospheric density
Beta-ray scattering
Density gauge

ABSTRACT

20. ABSTRACT (Continue on reverse side if necessary and identify by block number)

A density gauge for use in the 20-90 km range of the atmosphere was developed. It is based on beta-ray forward scattering and uses a Pm-147 beta source. Estimated accuracy is ±6% or better for launch on an Arcas having apogee near 90 km. The flight model will be ready for integration into the Arcas by March, 1978. A flight program for the sonde is recommended, and techniques offering potential for application of the method up to 100 km are discussed.

DD FORM 1 JAN 73 1473 EDITION OF 1 NOV 65 IS OBSOLETE

Unclassified

SECURITY CLASSIFICATION OF THIS PAGE (When Data Entered)

403 420 78 06 29 056

Foreword

The Betasonde was originally developed by Panametrics, Inc. under the sponsorship of the Division of Isotopes Development of the U. S. A. E. C. (Contract Monitor: Mr. John C. Dempsey) and the Atmospheric Sciences Branch of O. N. R. (Scientific Officer: Mr. James Hughes). Several launches of these early versions of the Betasonde were carried out at White Sands Missile Range, under the supervision of Mr. Harold N. Ballard of the Atmospheric Sciences Laboratory.

The advanced model Betasonde work reported here is supported by the Army Research Office and is monitored by Dr. Arthur V. Dodd of the Geosciences Division. The objective of the work is to develop a flight model of the Betasonde for integration into an Arcas rocket payload and application in a middle atmosphere flight program at White Sands Missile Range.

ACCESSION for
NTIS White Section
DDC Buff Section
UNANNOUNCED
JUSTIFICATION
BY
DISTRIBUTION/AVAILABILITY CODES
Dist. AVAIL. and/or SPECIAL
A

Table of Contents

List of Illustrations and Tables

1. Introduction

The Scope-of-Work for the subject contract is as follows:

The Contractor, as an independent Contractor and not as an agent of the Government, shall provide the necessary management, facilities, services and materials, as required, to accomplish the research project entitled "ATMOSPHERIC DENSITY MEASUREMENT IN THE MIDDLE ATMOSPHERE" in accordance with the Contractor's proposal dated November 1975 and revised during April 1976 which is incorporated as part of this contract by reference. The Contractor shall use the types of personnel listed in Exhibit A, attached, at approximately the level of effort stated. The research to be conducted will include but will not necessarily be limited to the design and fabrication of an instrument utilizing beta radiation to measure atmospheric density to an elevation of 100 kilometers. The first phase of the research involves investigation of satisfactory beta radiation sources and detection. Space simulation chambers will be used to measure and calculate the density response to beta radiation. Based on the results, a density sonde will be designed and fabricated in the second phase of the work.

Thus, the work under this contract is divided into two phases:

Phase I - Research and Development
Phase II - Design and Fabrication

If use is to be made of the Betasonde fabricated under Phase II, a third phase for flight and Data Analysis will have to be funded.

The objective of the present report is to summarize the Phase I effort that has taken place during the first year of the contract.

2. System Design

For Phase I, which is research and development work to determine optimum performance at altitudes up to 80 km, the system is designed for greatest flexibility. It consists of a basic betasonde with a charge preamplifier and of modular electronic units which are separate from the sonde. Since the modules have adjustable transfer functions, the system performance can be optimized very efficiently. The source-detector distance of the sonde is also adjustable to provide further flexibility.

The basic sonde configuration is shown in Fig. 2.1. A tripod-supported boom carries the annular beta source which irradiates the air volume in the

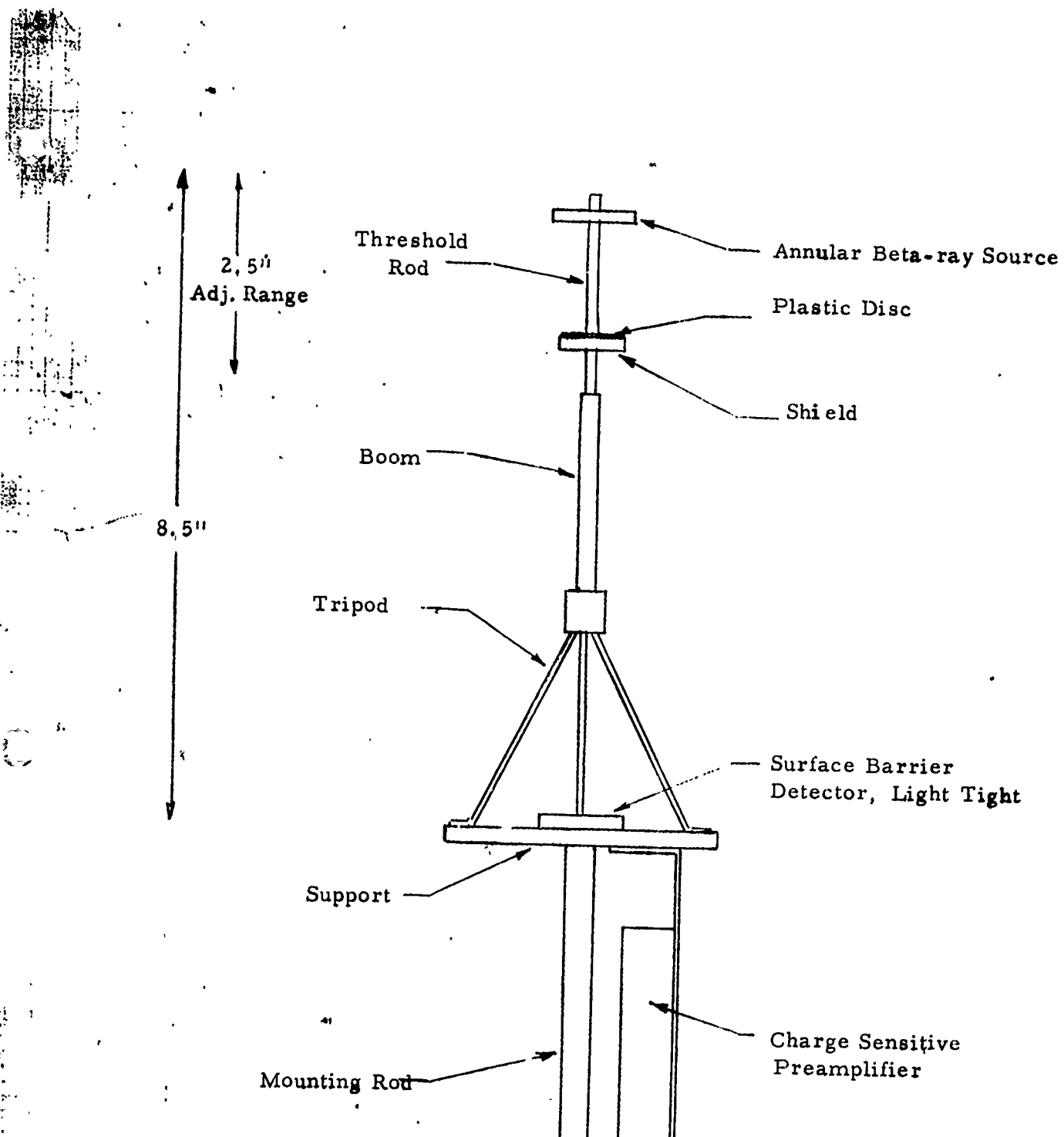

Figure 2.1. Betasonde II Laboratory Model

region between source and detector, outside the shield. The forward-scattered beta rays are detected by a surface barrier type semiconductor detector located at the base of the tripod. A shield is placed between the source and detector to prevent direct passage of beta particles from the source to the detector. A plastic disc is placed on the side of the shield that faces the source, in order to reduce bremsstrahlung generation. The distances of the source to the detectors and to the shield are independently adjustable to allow optimization of the system response characteristic. Included in this developmental sonde is a charge sensitive preamplifier which exhibits an extremely low noise haracteristic. Typically the noise is about 14 keV FWHM for a detector capacitance of 200 pf (approximate capacitance of detector to be used).

The detector is a ruggedized surface barrier type with an active area of 450 mm^2, sufficient to give a reasonable count rate up to an altitude of 80 km. Since a standard detector inherently responds to light in the visible spectrum, it is necessary for this application to have a specially processed detector featuring a light tight front surface. According to the manufacturer (Ortec, Inc.) a light tight front surface can be obtained with 120$\mu g/cm^2$ of aluminum, which is vapor deposited directly on the detector material. The latter is p-type silicon (rather than the standard n-type) in order for the aluminum to become the rectifying contact of the surface barrier diode, and thus the front of the detector. Other features of the detector are low noise (18 keV max for beta particles) and a depletion depth of 300μm at a bias of 100V. The relatively low bias voltage simplifies the design and assures low power dissipation of the bias power supply.

The original concept of the high-altitude Betasonde utilized an annular surface barrier detector with the source boom mounted through the center of that detector. Although this arrangement has the advantage of simpler mechanical construction, it has been found that the cost of a ruggedized, light weight, annular detector outweighs these advantages. The choice of the above described non-annular detector is based on its cost effectiveness and on the manufacturer's experience with the construction of such a special detector.

The output signal from the sonde's charge sensitive preamplifier is processed by modular electronics external to the vacuum chamber. A block diagram of the laboratory system is shown in Fig. 2.2. The voltage amplifier increases the pulse amplitude of the sonde's output signal to convenient values by means of its adjustable gain control. The trigger level of the threshold detector is set at a voltage equivalent to about 2.5 times the energy noise level of the detector. As stated above, the maximum noise

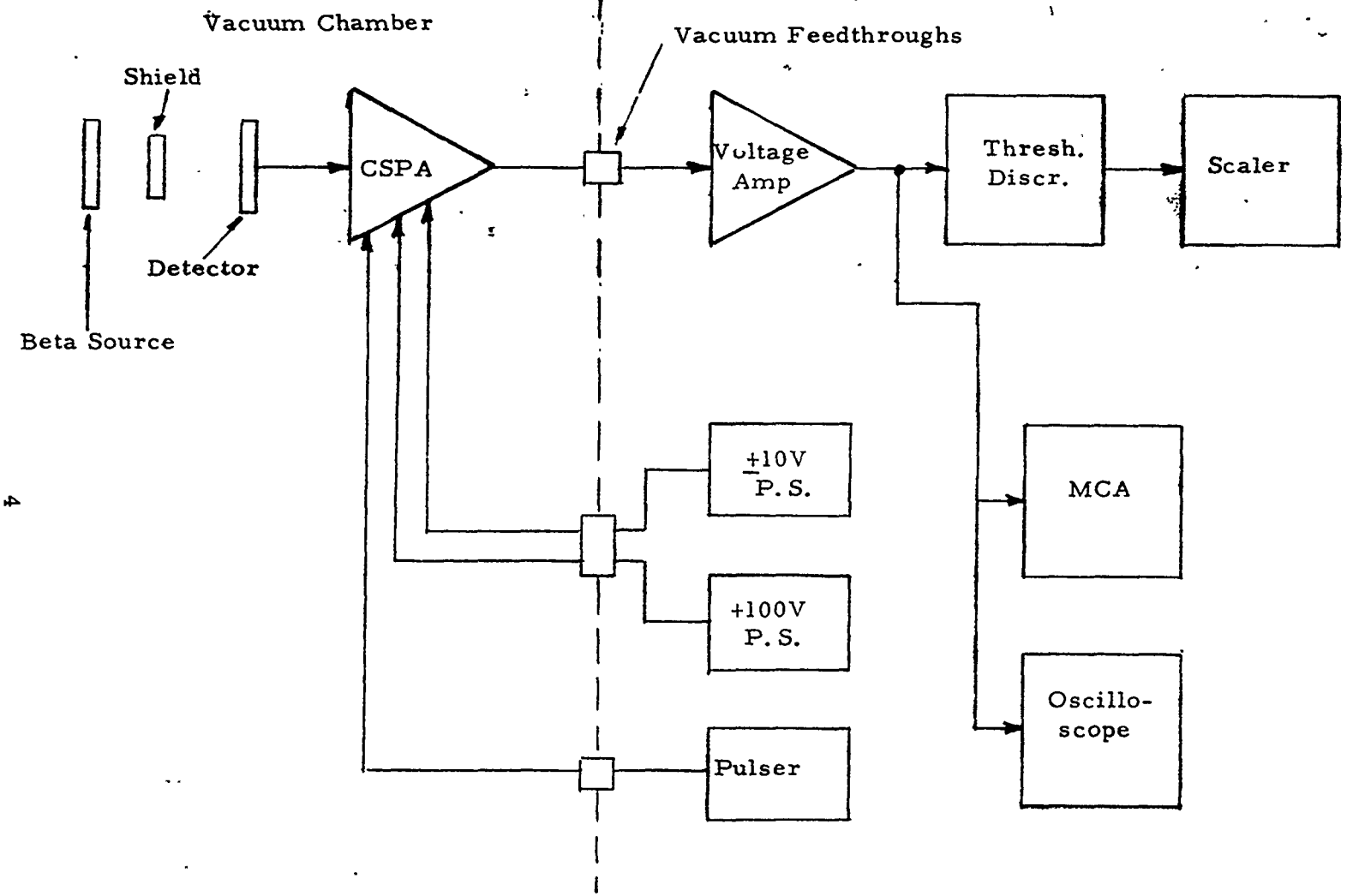

Figure 2.2 Block Diagram of Betasonde II Laboratory System

output from the detector is 18 keV which results in an energy threshold level of 45 keV. The sources suitable for investigation during this phase are: Pm-147, Sr-Y-90, Ni-63 and Tl-204. All have a high enough maximum energy that each spectrum contains a useful fraction of betas above the 45 keV threshold. The uniform pulses from the threshold detector are counted by the scaler. Thus, count rate data are obtained as a function of vacuum chamber pressure or by simple computation as a function of density.

For purposes of detector evaluation a multichannel analyzer (MCA) is included in the system. The MCA is used to determine the various source spectra. Available laboratory type power supplies are used to power the system.

3. Optimum Analytical Fit to Altitude-Density Profile

3.1 General Objective

As is well known, density $\rho(z)$ is approximately an exponentially decreasing function of altitude z:

$$\rho(z) = \rho_s e^{-z/H} \tag{3.1}$$

where H is the scale height and ρ_s the value of ρ at z=0. In fact, such an approximation is often made use of (Ref. 3.1, p 67) to provide analytical representations of models, for use in applications where such an approach is more convenient than is a long tabulation, for example where a computation is to be made that requires a continuous representation versus altitude. The result is generally provided in the form of the coefficients in a power series expansion for $\ell n \rho(z)$. We believe that a similar approach could also be useful for representing the data from a single determination of a $\rho(z)$ profile, in particular, from a rocket launch such as that of Betasonde II, the instrument being developed under the present contract for air density measurement up to at least 80 km by beta ray forward scattering.

The Low-Background Betasonde (LBB) is an earlier version Arcas borne instrument designed, principally, for measurement of $\rho(z)$ between about 25 and 65 km. The direct output of the data reduction procedure is a tabulation of individual densities $\rho_i(z)$ and associated statistical uncertainties, $\Delta\rho_i(z)$, versus z_i. When making use of data of this type it is normally not possible simply to interpolate directly between values in the tabulation. The reason is that the points, when plotted, will generally show an amount of scatter consistent with the uncertainties. Thus, in order to use such data it is necessary to draw a best-fit curve of some type on the plot (usually simply by eye). Values are then read off the curve and assumed to have an uncertainty consistent with that of the statistical $\Delta\rho_i(z)$, and any additional systematic errors, in that altitude region. Clearly, then, determination of an optimum analytical fit for a tabulation would serve two purposes. It would provide a "formal" method of fitting the data, and the resulting analytical fit would provide a convenient representation for computational purposes.

We will use the results of a launch of the LBB at White Sands Missile Range at 17:00:00 UT on April 23, 1976 (Ref. 3.2), to show the type analytical fit that can be obtained. First the general mathematical approach is presented, and this is followed by the density tabulation and the application of the approach to the tabulation to determine the optimum fit.

3.2 Mathematical Approach

The deviation of (3.1) from an exact exponential can be taken into account by allowing the scale height H to be a function of altitude. Over the altitude region up to about 100 km, H is not strongly dependent on z and should be representable as a simple function (this is essentially what is done in the standard approach to model fitting). By doing this the result H(z) is a physically meaningful parameter, although for a given analytical fit the dependence on z can be expected to agree with model results in only an approximate manner. For purposes of determining a fit over a particular altitude region it is then convenient, and appropriate, to use

$$\rho = \rho_o e^{-(z - z_o)/\bar{H}(z)} \tag{3.2}$$

where z_o is the (specified) minimum altitude of interest. ρ_o is the value of ρ at $z = z_o$ and $\bar{H}(z)$ is an "average" value of H(z), as determined by the fitting procedure. Thus, once ρ_o and $\bar{H}(z)$ are found from the procedure, the analytical result (3.2) represents the entire array of measured density profile data, which are in the form ρ_i and statistical uncertainty $\Delta\rho_i$ for all N altitudes z_i. The procedure is used to minimize the sum of the mean squared fractional deviations D_i of all ρ values, calculated from (3.2), from the measured results ρ_i:

$$D_i = (\rho - \rho_i)/\rho = 1 - \rho_i/\rho \tag{3.3}$$

Because $\bar{H}(z)$ occurs in the exponential, an exact minimization of this type would require solution of an array of non-linear equations. As we shall find, the maximum absolute values of D_i are about 0.1, in which case a very good approximation is

$$\ln(\rho/\rho_i) \approx 1 - \rho_i/\rho \tag{3.4}$$

For $|D_i| \leq .1$, the difference between the left and right hand sides of this equation never exceeds 5%.

Thus, we have used

$$D_i = \ln(\rho/\rho_i) \tag{3.5}$$

This expression, in itself, is completely valid for deriving a set of values of ρ_o and $\bar{H}(z)$ that provides a best fit to the experimental data; additionally, it gives a result that is very close to that which would be obtained from the exact fit, weighting large ($\approx .1$) deviations slightly less ($\approx 5\%$) than does the deviation (3.3).

In order to determine how well the fit has been made, once the procedure is complete, it is useful to compare two quantities. The first is the rms uncertainty Δ_m of the N values of fractional uncertainty Δ_i in the individual measurement,

$$\Delta_m^2 = \sum_{i=1}^{N} \Delta_i^2 / N \tag{3.6}$$

where

$$\Delta_i = \Delta\rho_i / \rho_i \tag{3.7}$$

and $\Delta\rho_i$ is the statistical uncertainty (Ref. 3.2, p 18). The second quantity is

$$\Delta_c^2 = \sum_i (\rho_i / \rho(z_i) - 1)^2 / N \tag{3.8}$$

which is the rms deviation of the $\rho(z_i)$ values, calculated by use of (3.2), from the measured values ρ_i. If all measurements were made at only one value of ρ, then it would be expected that $\Delta_m \approx \Delta_c$. This is because, for a given actual ρ, the random variations in the measured ρ_i for the Betasonde are due to the statistical nature of the nuclear decay process that leads to beta emission. The values of ρ_i are distributed in a Poisson-like manner, for which the fractional standard deviation of the mean of a series of N readings would be given by (3.6). The Pearson "chi-squared" test can readily be applied in such circumstances to determine how well the measurements fit the distribution assumed. Here, however, we are dealing with the comparison of a best analytical fit (rather than the mean of a series of measurements) to the individual measurements, each of which is expected to be slightly different because z is changing. Additionally, some atmospheric variability will exist that cannot be fitted by a simple function such as (3.2) without an unrealistically large amount of variation in $\bar{H}(z)$, and this will in itself cause Δ_c to exceed Δ_m. Clearly, in this case we expect $\Delta_c > \Delta_m$, and we can conclude that the fit is satisfactory if the difference is acceptably small.

Thus, the procedure here is to find the simplest possible representation of $\bar{H}(z)$ that will produce a value of Δ_c that is acceptably close to Δ_m. A fit in which $\Delta_c \ll \Delta_m$ would not represent a true best fit; this could be obtained by using a sufficiently complicated function for $\bar{H}(z)$ and would correspond to following the random deviations in the measurements, rather than the true average variation of $\rho(z)$. The question of exactly how closely Δ_c must approach Δ_m for the analytical fit to represent the experimental

tabulation acceptably is not considered further here. Rather, we shall show that fits can be obtained in which the difference is small and reduces in the manner expected as the number of A_j increases.

For use in the least square process, the quantity D_i from (3.5) is conveniently written

$$D_i = \ell n(1/\rho_i) - \ell n(1/\rho) \tag{3.9}$$

We will represent $\bar{H}(z)$ by an inverse power series with coefficients A_j, so that from (3.2) we have,

$$\ell n(1/\rho) = \ell n(1/\rho_o) + (z - z_o)/\bar{H}(z) \tag{3.10}$$

$$= \sum_{j=1}^{j_m} A_j (z - z_o)^{j-1} \tag{3.11}$$

where

$$\ell n(1/\rho_o) = A_1 \tag{3.12}$$

$$(z - z_o)/\bar{H}(z) = \sum_{j=2}^{j_m} A_j (z - z_o)^{j-1} \tag{3.13}$$

and j_m is the number of coefficients A_j chosen to be used. Clearly, once all A_j in the single power series (3.11) are known, both ρ_o and $\bar{H}(z)$ can be found from (3.12) and (3.13):

$$\rho_o = e^{-A_1} \tag{3.14}$$

$$\bar{H}(z) = 1 \Big/ \sum_{j=2}^{j_m} A_j (z - z_o)^{j-2} \tag{3.15}$$

Hence, a fit must be made to $\ell n(1/\rho)$ to determine the A_j from (3.11) for use in (3.14) and (3.15), which then defines $\rho(z)$ from (3.2).

The approach used is a standard least square procedure. The total squared deviation for all N measured values of ρ_i, and associated uncertainties $\Delta\rho_i$, at altitude z_i is given by use of (3.9) and (3.10) as

$$\Delta^2 = \sum_{i=1}^{N} w_i D_i^2$$

$$= \sum_i w_i \left(f_i - \sum_{j=1}^{j_m} A_j h_i^{j-1} \right)^2 \qquad (3.16)$$

where

$$h_i = z_i - z_o \qquad (3.17)$$

and

$$f_i = \ell n(1/\rho_i). \qquad (3.18)$$

The weights w_i are taken as inversely proportional to the squared fractional uncertainties Δ_i,

$$w_i = 1/\left(W\Delta_i^2\right) \qquad (3.19)$$

where Δ_i is given by (3.7) and the normalization constant W is chosen, for convenience, so that

$$\sum w_i = 1, \qquad (3.20)$$

which defines W from (3.19) as

$$W = \sum_i \left(1/\Delta_i^2\right). \qquad (3.21)$$

The weighting (3.19) thus gives most importance to those measurements for which the fractional uncertainties are small; but none of the Δ_i may be zero, of course, since this would imply that that particular ρ_i is known exactly.

The least square procedure then proceeds by requiring that for each particular one of the A_j, say A_k,

$$\frac{\partial \Delta^2}{\partial A_k} = 0; \; k = 1 \text{ to } j_m \qquad (3.22)$$

which, by use of (3.16), yields j_m linear equations for the A_j of the form:

$$V_k = \sum_{j=1}^{j_m} B_{kj} A_j; \quad k = 1 \text{ to } j_m \tag{3.23}$$

where,

$$V_k = \sum_{i=1}^{N} w_i f_i h_i^{k-1} \tag{3.24}$$

and

$$B_{kj} = \sum_{j=1}^{N} w_i h_i^{k+j-2} \tag{3.25}$$

Thus, given a set of N values of ρ_i, Δ_i and z_i, the quantities f_i, h_i and w_i are found from (3.18), (3.17) and (3.19), the number j_m of coefficients A_j to be used for the fit is chosen, and the values of V_k and B_{kj} are determined from (3.24) and (3.25) for k and j = 1 to j_m. These values are then used in the j_m equations (3.23), and the A_j are determined by solution of that set of linear equations.

Model fitting often requires use of 10 to 14 coefficients in a similar procedure to obtain what is considered to be an adequate fit. Here we will find that for the particular experimental data used, 4 or 5 are sufficient to provide a fit whose accuracy is consistent with the accuracy of the data. Thus, after the fitting procedure is completed for each particular value of j_m, the value of Δ_c is found from (3.8) and compared with Δ_m from (3.6) to determine the adequacy of the fit.

3.3 Flight Data and Density Tabulation

Details of the Low Background Betasonde (LBB) flight on April 23, 1976 are contained in Ref. 3.2 and presented here only to the extent necessary for application of the above procedure.

The Arcas was launched to an apogee altitude near 65 km, with the parachute borne LBB being ejected just before apogee. The parachute has little effect above 50 km. The descent velocity changes from about .2 km/sec to .02 km/sec between 60 and 30 km. However, the sonde does spend nearly 20 seconds within 1 km of apogee, thus providing much data in this region before beginning its rapid descent. This is an important fact,

because it allows the density profile to be "tied down" at high altitude. Clearly, as the sonde descent rate slows, it obtains progressively more data in each altitude region. Hence, the entire density profile for the low altitude region is very accurately defined. The procedure described above is designed such that it provides a single analytical fit that automatically takes all of these factors into account.

The Betasonde pulses, each of which (except for cosmic ray background) corresponds to detection of an air-scattered beta particle, are telemetered and recorded on magnetic tape in real-time. These pulses are then summed into approximately equal time intervals t_m - depending upon telemetry noise and time used for transmitting temperature for diagnostic purposes. In Table 3.1 these sums are labelled CTS at each altitude z(km) for the time interval TM(SECS). These are the basic flight data from which the density measurement at each altitude is determined.

It is seen that the counts generally increase as altitude decreases, because the number of beta particles scattered increases as the density increases in this density region. In addition to the density itself, there are several other factors that must be taken into account in determining density from this count rate:

1) circuit dead-time, caused by dead time in geiger counters after counting a pulse ($\approx 25\mu$sec) and a dead-time circuit introduced purposely to keep the count rate into the telemetry transmitter from exceeding its capabilities,

2) cosmic ray effect, a small, but non-negligible, altitude dependent effect,

and 3) time elapsed between calibration and flight.

Each of these factors has been taken into account as necessary in obtaining the calibration data of Table 3.2 and the flight density tabulation in Table 3.3. In the latter table the count data from Table 3.1 are repeated as the first three columns, with the observed counts (OBSCTS) in the third. This leads to an observed count rate (not shown) which is corrected for dead time, by use of the circuit dead time of 185μsec, to obtain the corrected count rate (CORCTR). The cosmic ray count rate (COSCTR) is then subtracted to obtain the density-dependent count rate (DENCTR). The DENSITY (g/m^3) ρ_i for the altitude z_i is then determined by use of the calibration results of Table 3.2, and the absolute uncertainty, UNC(g/m^3) from the density, the counts, and the calibration data. The fractional uncertainty Δ_i is given by the ratio UNC/DENSITY.

Table 3.1 Low Background Betasonde Count Data for April 23, 1976 Flight

Z(KM)	TM(SECS)	CTS
64.0	5.5	80.
64.3	5.2	89.
64.2	5.4	85.
63.5	5.2	83.
62.9	5.1	102.
62.1	5.1	99.
61.0	5.2	130.
60.0	5.2	133.
59.1	5.1	156.
57.9	5.1	155.
55.9	5.1	219.
54.9	5.1	240.
53.9	5.1	259.
53.0	5.1	279.
52.0	5.0	355.
51.2	5.2	376.
50.5	5.0	376.
50.0	4.1	311.
49.5	4.0	361.
48.6	5.0	543.
48.1	5.0	502.
47.7	5.1	565.
47.2	4.0	467.
46.8	4.0	485.
46.4	4.1	495.
45.8	2.0	307.
45.3	4.0	650.
45.0	4.0	626.
44.2	4.0	683.
43.9	4.0	748.
43.4	5.0	1047.
43.1	5.1	989.
42.8	5.0	1093.
42.5	5.0	1124.
42.2	5.1	1197.
41.9	4.0	942.
41.7	4.0	1024.
41.1	5.0	1408.
40.8	5.0	1443.
40.5	5.0	1510.
40.2	5.1	1538.
40.0	5.0	1610.
39.7	5.0	1652.
39.5	5.0	1742.
39.3	5.0	1803.
39.0	4.0	1507.
38.5	4.1	1574.
38.3	5.0	2007.
38.1	5.0	2086.
37.9	5.0	2228.
37.6	5.0	2241.
37.4	5.0	2335.
37.2	5.0	2385.
37.0	5.0	2400.
36.8	5.0	2545.
36.2	5.0	2808.
36.1	5.0	2964.
35.9	5.0	2975.
35.7	5.0	2890.
35.5	5.0	3102.
35.4	5.0	3098.
35.2	5.0	3166.
35.1	5.0	3344.
34.9	4.0	2655.
34.5	5.1	3547.
34.4	5.0	3628.
34.3	5.0	3530.
34.1	5.0	3444.
34.0	5.0	3666.
33.9	5.0	3809.
33.7	5.0	3829.
33.6	5.0	4038.
33.5	4.0	3283.
33.1	5.0	4097.
33.0	5.1	4227.
32.9	5.0	4359.
32.8	5.0	4363.
32.6	5.0	4580.
32.4	5.0	4735.
32.2	5.0	4755.
32.1	5.0	4895.
32.0	4.0	3944.
31.6	5.0	5055.
31.5	5.0	5353.
31.3	5.1	5316.
31.2	5.0	5271.
31.0	5.0	5406.
30.8	5.0	5701.
30.7	5.0	5707.
30.5	5.0	5901.
30.4	4.0	4735.
30.0	5.0	6338.
29.9	5.0	6418.
29.7	5.0	6332.
29.6	5.0	6350.
29.5	5.0	6462.
29.3	5.0	6764.
29.1	5.0	6708.
29.0	5.0	6757.
28.9	4.0	5757.
28.6	5.0	6895.
28.5	5.1	7383.
28.3	5.0	7335.
28.2	5.0	7454.
28.1	5.0	7724.
27.9	5.0	7764.
27.7	5.0	7901.
27.6	5.0	7778.
27.4	4.0	6502.
27.2	5.0	8424.
27.1	4.0	6541.
27.0	5.0	8401.
26.9	5.0	8239.
26.7	5.0	8719.
26.6	5.0	8675.
26.5	5.1	8509.
26.3	5.0	8914.
26.2	5.0	8892.

Table 3.2 Low Background Betasonde Density Calibration Data Recorded April 7, 1976.

PT	RHO(G/M**3)	CTS/SEC
01	00	0000.
02	02	0174.
03	04	0352.
04	06	0524.
05	08	0700.
06	10	0874.
07	12	1045.
08	14	1220.
09	16	1400.
10	18	1575.
11	20	1750.
12	22	1900.
13	24	2020.
14	26	2130.
15	28	2245.
16	30	2345.
17	32	2440.
18	34	2530.
19	36	2620.
20	38	2705.
21	40	2790.
22	42	2880.

Table 3.3 Low Background Betasonde Measured Density Tabulation for April 23, 1976 Flight

MEAN-LIFE,DAYS=1378.
TIME FROM CAL,DAYS=16.
CIR. DEAD TIME,SEC=.000185

UNITS:ALT=KM;TIME-INT=SEC;ALL CTR=CPS;DEN,UNC=G/M**3

ALT	TIME-INT	OBSCTS	CORCTR	COSCTR	DENCTR	DENSITY	UNC FRAC-UNC	
64.0	5.5	80.	14.58	0.30	14.45	0.168	0.019	0.112
64.3	5.2	89.	17.17	0.30	17.07	0.198	0.021	0.106
64.2	5.4	85.	15.79	0.30	15.67	0.182	0.020	0.108
63.5	5.2	83.	16.01	0.30	15.89	0.185	0.020	0.110
62.9	5.1	102.	20.07	0.30	20.01	0.232	0.023	0.099
62.1	5.1	99.	19.48	0.30	19.41	0.225	0.023	0.100
61.0	5.2	130.	25.12	0.30	25.11	0.291	0.026	0.088
60.0	5.2	133.	25.70	0.30	25.70	0.298	0.026	0.087
59.1	5.1	156.	30.76	0.30	30.82	0.357	0.029	0.080
57.9	5.1	155.	30.56	0.30	30.62	0.355	0.028	0.080
55.9	5.1	219.	43.29	0.30	43.49	0.504	0.034	0.067
54.9	5.1	240.	47.47	0.30	47.72	0.553	0.036	0.064
53.9	5.1	259.	51.27	0.30	51.56	0.597	0.037	0.062
53.0	5.1	279.	55.27	0.30	55.61	0.644	0.038	0.060
52.0	5.0	355.	71.94	0.30	72.48	0.839	0.044	0.053
51.2	5.2	376.	73.29	0.30	73.84	0.854	0.044	0.051
50.5	5.0	376.	76.26	0.30	76.85	0.889	0.046	0.051

Table 3.3 (Cont.)

ALT	TIME-INT	OBSCTS	CORCTR	COSCTR	DENCTR	DENSITY	UNC	FRAC-UNC
50.0	4.1	311.	76.93	0.30	77.53	0.897	0.051	0.056
49.5	4.0	361.	91.78	0.31	92.54	1.069	0.056	0.052
48.6	5.0	543.	110.83	0.32	111.80	1.290	0.055	0.043
48.1	5.0	502.	102.30	0.32	103.17	1.191	0.053	0.044
47.7	5.1	565.	113.10	0.33	114.09	1.316	0.055	0.042
47.2	4.0	467.	119.33	0.33	120.38	1.388	0.064	0.046
46.8	4.0	485.	124.03	0.34	125.14	1.443	0.065	0.045
46.4	4.1	495.	123.49	0.34	124.58	1.437	0.064	0.045
45.8	2.0	307.	157.99	0.35	159.48	1.835	0.104	0.056
45.3	4.0	650.	167.54	0.36	169.13	1.945	0.075	0.039
45.0	4.0	626.	161.17	0.36	162.68	1.871	0.074	0.040
44.2	4.0	683.	176.32	0.37	178.00	2.044	0.075	0.037
43.9	4.0	748.	193.70	0.37	195.58	2.239	0.079	0.035
43.4	5.0	1047.	217.84	0.38	220.00	2.510	0.076	0.030
43.1	5.1	989.	201.14	0.38	203.10	2.322	0.072	0.031
42.8	5.0	1093.	227.81	0.39	230.08	2.622	0.078	0.030
42.5	5.0	1124.	234.55	0.39	236.90	2.699	0.079	0.029
42.2	5.1	1197.	245.36	0.40	247.82	2.821	0.080	0.028
41.9	4.0	942.	246.23	0.40	248.70	2.831	0.091	0.032
41.7	4.0	1024.	268.73	0.40	271.46	3.086	0.095	0.031
41.1	5.0	1408.	297.08	0.41	300.13	3.410	0.091	0.027
40.8	5.0	1443.	304.88	0.41	308.02	3.499	0.092	0.026
40.5	5.0	1510.	319.87	0.42	323.19	3.671	0.095	0.026
40.2	5.1	1538.	319.39	0.42	322.69	3.666	0.094	0.026
40.0	5.0	1610.	342.40	0.42	345.97	3.931	0.098	0.025
39.7	5.0	1652.	351.91	0.43	355.59	4.042	0.103	0.025
39.5	5.0	1742.	372.40	0.43	376.32	4.285	0.106	0.025
39.3	5.0	1803.	386.38	0.43	390.45	4.451	0.108	0.024
39.0	4.0	1507.	404.98	0.43	409.27	4.671	0.123	0.026
38.5	4.1	1574.	413.25	0.44	417.63	4.768	0.123	0.026
38.3	5.0	2007.	433.60	0.44	438.21	5.008	0.114	0.023
38.1	5.0	2086.	452.09	0.45	456.92	5.225	0.116	0.022
37.9	5.0	2228.	485.63	0.45	490.85	5.618	0.120	0.021
37.6	5.0	2241.	488.72	0.45	493.97	5.654	0.120	0.021
37.4	5.0	2335.	511.16	0.45	516.67	5.916	0.123	0.021
37.2	5.0	2385.	523.17	0.46	528.81	6.054	0.122	0.020
37.0	5.0	2400.	526.78	0.46	532.47	6.096	0.123	0.020
36.8	5.0	2545.	561.91	0.46	568.01	6.498	0.128	0.020
36.2	5.0	2808.	626.71	0.47	633.56	7.242	0.136	0.019
36.1	5.0	2964.	665.82	0.47	673.12	7.693	0.141	0.018
35.9	5.0	2975.	668.60	0.47	675.93	7.725	0.141	0.018
35.7	5.0	2890.	647.21	0.48	654.28	7.478	0.139	0.019
35.5	5.0	3102.	700.84	0.48	708.54	8.097	0.145	0.018
35.4	5.0	3098.	699.82	0.48	707.51	8.086	0.145	0.018
35.2	5.0	3166.	717.22	0.48	725.11	8.286	0.147	0.018
35.1	5.0	3344.	763.23	0.48	771.66	8.819	0.153	0.017
34.9	4.0	2655.	756.66	0.49	765.01	8.743	0.170	0.019
34.5	5.1	3547.	798.19	0.49	807.02	9.226	0.156	0.017
34.4	5.0	3628.	838.10	0.49	847.39	9.692	0.163	0.017
34.3	5.0	3530.	812.06	0.49	821.05	9.388	0.159	0.017
34.1	5.0	3444.	789.39	0.50	798.11	9.123	0.156	0.017

Table 3.3 (Cont.)

ALT	TIME-INT	OBSCTS	CORCTR	COSCTR	DENCTR	DENSITY	UNC	FRAC-UNC
34.0	5.0	3666.	848.26	0.50	857.66	9.811	0.164	0.017
33.9	5.0	3809.	886.78	0.50	896.63	10.267	0.171	0.017
33.7	5.0	3829.	892.20	0.50	902.11	10.332	0.172	0.017
33.6	5.0	4038.	949.45	0.50	960.04	11.012	0.177	0.016
33.5	4.0	3283.	967.68	0.50	978.47	11.227	0.199	0.018
33.1	5.0	4097.	965.81	0.51	976.57	11.205	0.178	0.016
33.0	5.1	4227.	978.92	0.51	989.84	11.360	0.177	0.016
32.9	5.0	4359.	1039.44	0.51	1051.07	12.070	0.184	0.015
32.8	5.0	4363.	1040.58	0.51	1052.22	12.084	0.184	0.015
32.6	5.0	4580.	1102.90	0.51	1115.26	12.810	0.189	0.015
32.4	5.0	4735.	1148.15	0.52	1161.04	13.332	0.192	0.014
32.2	5.0	4755.	1154.04	0.52	1166.99	13.400	0.192	0.014
32.1	5.0	4895.	1195.53	0.52	1208.96	13.876	0.195	0.014
32.0	4.0	3944.	1205.98	0.52	1219.54	13.995	0.219	0.016
31.6	5.0	5055.	1243.60	0.53	1257.59	14.413	0.195	0.014
31.5	5.0	5353.	1335.01	0.53	1350.07	15.439	0.206	0.013
31.3	5.1	5316.	1291.38	0.53	1305.92	14.947	0.199	0.013
31.2	5.0	5271.	1309.61	0.53	1324.37	15.153	0.203	0.013
31.0	5.0	5406.	1351.54	0.53	1366.78	15.627	0.208	0.013
30.8	5.0	5701.	1445.00	0.54	1461.34	16.701	0.221	0.013
30.7	5.0	5707.	1446.93	0.54	1463.29	16.723	0.221	0.013
30.5	5.0	5901.	1509.86	0.54	1526.95	17.451	0.227	0.013
30.4	4.0	4735.	1515.67	0.54	1532.83	17.518	0.255	0.015
30.0	5.0	6338.	1655.92	0.55	1674.71	19.096	0.243	0.013
29.9	5.0	6418.	1683.33	0.55	1702.44	19.421	0.253	0.013
29.7	5.0	6332.	1653.88	0.55	1672.64	19.072	0.243	0.013
29.6	5.0	6350.	1660.02	0.55	1678.85	19.144	0.245	0.013
29.5	5.0	6462.	1698.50	0.55	1717.78	19.605	0.258	0.013
29.3	5.0	6764.	1804.38	0.55	1824.89	20.929	0.296	0.014
29.1	5.0	6708.	1784.51	0.56	1804.79	20.666	0.283	0.014
29.0	5.0	6757.	1801.89	0.56	1822.37	20.896	0.294	0.014
28.9	4.0	5757.	1961.53	0.56	1983.87	23.378	0.444	0.019
28.6	5.0	6895.	1851.29	0.56	1872.34	21.589	0.327	0.015
28.5	5.1	7383.	1977.16	0.56	1999.68	23.648	0.400	0.017
28.3	5.0	7335.	2013.44	0.57	2036.38	24.303	0.439	0.018
28.2	5.0	7454.	2058.54	0.57	2082.01	25.138	0.437	0.017
28.1	5.0	7724.	2162.94	0.57	2187.63	26.962	0.433	0.016
27.9	5.0	7764.	2178.66	0.57	2203.53	27.242	0.445	0.016
27.7	5.0	7901.	2232.98	0.57	2258.48	28.263	0.498	0.018
27.6	5.0	7778.	2184.17	0.57	2209.10	27.341	0.449	0.016
27.4	4.0	6502.	2324.53	0.58	2351.09	30.125	0.599	0.020
27.2	5.0	8424.	2447.73	0.58	2475.73	32.794	0.599	0.018
27.1	4.0	6541.	2344.52	0.58	2371.31	30.542	0.609	0.020
27.0	5.0	8401.	2438.03	0.58	2465.91	32.576	0.598	0.018
26.9	5.0	8239.	2370.40	0.58	2397.49	31.091	0.558	0.018
26.7	5.0	8719.	2574.27	0.59	2603.74	35.629	0.632	0.018
26.6	5.0	8675.	2555.13	0.59	2584.38	35.194	0.620	0.018
26.5	5.1	8509.	2413.33	0.59	2440.92	32.020	0.588	0.018
26.3	5.0	8914.	2660.17	0.59	2690.64	37.662	0.671	0.018
26.2	5.0	8892.	2650.39	0.59	2680.74	37.429	0.669	0.018

The last of the factors that must be taken into account is important because of decay in intensity of the radioactive source, in this case Pm-147 whose mean life is 1378 days. Essentially, a calibration curve that would be correct on the day of the flight is derived from that recorded earlier. In the present instance the time lapse was only 16 days, and the calibration data are shown in Table 3.2. There are 22 points at which the density $\rho(g/m^3)$ and the count rate, corrected for the dead time factor, was as shown in CTS/SEC. At low values of ρ the count rate increases approximately linearly, but as ρ increases the count rate increases less rapidly. At 25 km $\rho \approx 40$ g/m^3 and at 30 km $\rho \approx 20$ g/m^3. Data below about 30 km were not analyzed in Ref. 3.1 because of the non-linear nature of the calibration curve in that region. Here, however, all of the data in Table 3.1 are analyzed. This was done by making, for each flight count rate, a quadratic fit to three appropriate calibration count rate points in Table 3.2. The measured DENSITY values of Table 3.3 were thus determined from that analytical fit to the density - count rate results in Table 3.2.

The array of 118 altitudes z_i, measured densities ρ_i and fractional statistical uncertainties Δ_i given in Table 3.3 are the input data for the least square mathematical procedure described in Section 3.2.

3.4 Results of Analytical Fit for April 23, 1976 Low Background Betasonde Flight

By use of the data in Table 3.3 for z_i, ρ_i and Δ_i, Eqs. (3.23) were solved for j_m = 2-5 to obtain the values for the coefficients A_j. For each set of solutions the results for rms sum of the weighted deviations between the analytical fit and experimental points was determined from (3.16). This is the quantity that was minimized to produce the solution obtained. Δ_c, the rms unweighted deviation sum, was also calculated from (3.8); both Δ and Δ_c are to be compared to Δ_m, the rms fractional uncertainty, from (3.6). Results for all of these parameters, along with ρ_o from (3.14), are given in Table 3.4.

The rms fractional uncertainty, Δ_m, is independent of j_m and has the value 0.039. As noted above, a satisfactory fit is one in which the difference between Δ_c and Δ_m is acceptably small.

As seen from the table, Δ decreases rapidly as j_m goes from 2 to 3, but with j_m as large as 5 the accuracy of the fit is marginally better. Δ_c appears to go thru a minimum at $j_m = 4$. As observed above, a fit derived by minimizing Δ, the rms sum of the deviations weighted inversely with the uncertainties, is taken here as the proper procedure to follow. This causes those points with most accuracy to produce the most effect on the fit. However, such a fit should not be allowed to produce a large value of

Table 3.4 Parametric Results of Analytical Fit for LBB Flight on April 23, 1976

Δ_m = .03909, z_o = 26.2 km

j_m	A_1	A_2	A_3	A_4	A_5	$\rho_o(g/m^3)$	Δ	Δ_c
2	-.35136+1	+.15248+0	-	-	-	33.568	.05709	.21408
3	-.35771+1	+.17100+0	-.84900-3	-	-	35.770	.03723	.04505
4	-.35753+1	+.17017+0	-.76747-3	-.18776-5	-	35.707	.03722	.04475
5	-.35864+1	+.17821+0	-.21034-2	+.69676-4	-.11369-5	36.104	.03675	.04921

Read $N\pm n$ as $N \times 10^{\pm n}$ for all A_j

Summed over entire altitude range:

Δ_m = RMS fractional statistical uncertainty in measured density, Eq. (3.6).

Δ = RMS value of approximate difference D_i [Eq. (3.5)] between measured and fit-calculated densities, weighted inversely with fractional statistical uncertainty in measured density, Eq. (3.16).

Δ_c = RMS value of actual difference D_i [Eq. (3.3)] between measured and fit-calculated densities, unweighted, Eq. (3.8).

Δ_c, the rms sum of the unweighted deviations. In view of the fact that there is undoubtedly some short-term atmospheric variability in density, it is unlikely that a fit in which Δ_c approaches Δ_m much more closely than in the present case would be expected. Thus, in the present instance at least, a criterion for selecting the most satisfactory of the fits obtained by minimizing Δ, is that particular one for which Δ_c is a minimum; $j_m = 4$ here. Whether such a dependence on j_m will always occur is not presently known. When the results of additional flights are available, further investigation of the method of selecting the optimum fit should be made.

The quantity $\bar{H}(z)$ given by (3.15) is actually to be used in (3.2) to provide the optimum analytical fit to the data. However, for purposes of comparison with models it is useful to have the value of H(z). This can be determined as follows. Note from (3.1) that

$$H(z) = -1 \Big/ \left(\frac{d\rho/\rho}{dz}\right) \tag{3.26}$$

But, from (3.2) for the fit used here this gives

$$H(z) = 1 \Big/ \frac{d}{dz}\left(\frac{z - z_o}{\bar{H}(z)}\right) \tag{3.27}$$

Use of (3.15) then yields

$$H(z) = 1 \Big/ \sum_{j=2}^{j_m} A_j (j-1)(z-z_o)^{j-2} \tag{3.28}$$

Consequently, once the A_j have been determined it is possible to calculate the value of H(z) as well as $\bar{H}(z)$.

For the fit with $j_m = 4$, results are given in Table 3.5 and Figures 3.1 and 3.2. The first three columns of the table give z_i, ρ_i and $\Delta\rho_i$ (ALT, DENSITY and UNC in Table 3.3). The next three give $\rho(z)$, $\bar{H}(z)$, and H(z) as calculated from (3.2), (3.15), and (3.28), respectively. The next column gives the fractional difference between measured ρ_i and calculated $\rho(z)$. The final column, labeled RMS FRAC, is a running rms average of the fractional difference for that altitude with that of the four previous (higher altitude points). Hence, it is assigned the value zero for the four highest altitude points.

Table 3.5 Altitude Dependence Results of Analytical Fit for LBB Flight on April 23, 1976

$j_m = 4$

RESULTS OF FIT

J	A(J)
1	-0.35753E+01
2	0.17017E+00
3	-0.76747E-03
4	-0.18776E-05

Z0= 26.2 KM
RHO0= 35.707 G/M**3

RMS FRAC=RMS AVG OF PREV 5 DIFF FRACS

ALT KM	RHO-MEAS G/M**3	UNCER G/M**3	RHO-CALC G/M**3	HBAR(Z) KM	H(Z) KM	DIFF FRAC	RMS FRAC
64.0	0.168	0.019	0.190	7.221	9.606	-0.117	0.000
64.3	0.198	0.021	0.184	7.236	9.661	0.073	0.000
64.2	0.182	0.020	0.186	7.231	9.642	-0.024	0.000
63.5	0.185	0.020	0.201	7.198	9.516	-0.077	0.000
62.9	0.232	0.023	0.214	7.170	9.412	0.086	0.081
62.1	0.225	0.023	0.233	7.133	9.276	-0.033	0.064
61.0	0.291	0.026	0.262	7.083	9.096	0.109	0.073
60.0	0.298	0.026	0.293	7.038	8.940	0.017	0.073
59.1	0.357	0.029	0.324	6.998	8.805	0.100	0.078
57.9	0.355	0.028	0.372	6.947	8.632	-0.046	0.071
55.9	0.504	0.034	0.471	6.862	8.360	0.070	0.077
54.9	0.553	0.036	0.532	6.821	8.232	0.040	0.062
53.9	0.597	0.037	0.601	6.781	8.108	-0.006	0.061
53.0	0.644	0.038	0.672	6.745	8.001	-0.041	0.046
52.0	0.839	0.044	0.762	6.706	7.885	0.101	0.061
51.2	0.854	0.044	0.844	6.675	7.796	0.012	0.052
50.5	0.889	0.046	0.923	6.648	7.719	-0.037	0.052
50.0	0.897	0.051	0.985	6.629	7.666	-0.090	0.066
49.5	1.069	0.056	1.052	6.611	7.613	0.016	0.063
48.6	1.290	0.055	1.185	6.577	7.521	0.089	0.060
48.1	1.191	0.053	1.267	6.559	7.471	-0.060	0.065
47.7	1.316	0.055	1.337	6.544	7.431	-0.015	0.063
47.2	1.388	0.064	1.430	6.526	7.383	-0.029	0.051
46.8	1.443	0.065	1.510	6.512	7.344	-0.044	0.054
46.4	1.437	0.064	1.594	6.498	7.306	-0.099	0.057
45.8	1.835	0.104	1.731	6.476	7.250	0.060	0.057
45.3	1.945	0.075	1.855	6.459	7.205	0.048	0.061
45.0	1.871	0.074	1.935	6.448	7.178	-0.033	0.061
44.2	2.044	0.075	2.164	6.421	7.106	-0.055	0.063
43.9	2.239	0.079	2.257	6.410	7.080	-0.008	0.045
43.4	2.510	0.076	2.423	6.393	7.037	0.036	0.040
43.1	2.322	0.072	2.529	6.383	7.012	-0.082	0.049

Table 3.5 (cont'd)

ALT KM	RHO-MEAS G/M**3	UNCER G/M**3	RHO-CALC G/M**3	HBAR(Z) KM	H(Z) KM	DIFF FRAC	RMS FRAC
42.8	2.622	0.078	2.639	6.373	6.986	-0.007	0.047
42.5	2.699	0.079	2.755	6.363	6.961	-0.021	0.041
42.2	2.821	0.080	2.877	6.353	6.936	-0.019	0.042
41.9	2.831	0.091	3.004	6.343	6.912	-0.058	0.047
41.7	3.086	0.095	3.093	6.336	6.895	-0.002	0.029
41.1	3.410	0.091	3.375	6.316	6.847	0.010	0.029
40.8	3.499	0.092	3.526	6.307	6.823	-0.008	0.028
40.5	3.671	0.095	3.685	6.297	6.800	-0.004	0.027
40.2	3.666	0.094	3.852	6.287	6.776	-0.048	0.022
40.0	3.931	0.098	3.967	6.281	6.761	-0.009	0.023
39.7	4.042	0.103	4.148	6.271	6.738	-0.025	0.025
39.5	4.285	0.106	4.273	6.264	6.722	0.003	0.025
39.3	4.451	0.108	4.402	6.258	6.707	0.011	0.025
39.0	4.671	0.123	4.604	6.248	6.684	0.015	0.015
38.5	4.768	0.123	4.962	6.233	6.647	-0.039	0.022
38.3	5.008	0.114	5.114	6.226	6.632	-0.021	0.021
38.1	5.225	0.116	5.271	6.220	6.618	-0.009	0.022
37.9	5.618	0.120	5.433	6.214	6.603	0.034	0.026
37.6	5.654	0.120	5.685	6.204	6.582	-0.006	0.025
37.4	5.916	0.123	5.861	6.198	6.567	0.009	0.019
37.2	6.054	0.122	6.043	6.192	6.553	0.002	0.017
37.0	6.096	0.123	6.230	6.186	6.539	-0.022	0.019
36.8	6.498	0.128	6.424	6.180	6.525	0.012	0.012
36.2	7.242	0.136	7.045	6.161	6.483	0.028	0.017
36.1	7.693	0.141	7.154	6.158	6.476	0.075	0.038
35.9	7.725	0.141	7.379	6.152	6.462	0.047	0.043
35.7	7.478	0.139	7.611	6.146	6.448	-0.017	0.043
35.5	8.097	0.145	7.851	6.140	6.435	0.031	0.045
35.4	8.085	0.145	7.974	6.137	6.428	0.014	0.043
35.2	8.286	0.147	8.226	6.131	6.414	0.007	0.027
35.1	8.819	0.153	8.356	6.128	6.408	0.055	0.030
34.9	8.743	0.170	8.621	6.122	6.394	0.014	0.030
34.5	9.226	0.156	9.179	6.110	6.368	0.005	0.027
34.4	9.692	0.163	9.324	6.107	6.361	0.039	0.031
34.3	9.388	0.159	9.472	6.104	6.355	-0.009	0.031
34.1	9.123	0.156	9.775	6.098	6.341	-0.067	0.036
34.0	9.811	0.164	9.930	6.095	6.335	-0.012	0.035
33.9	10.267	0.171	10.088	6.092	6.328	0.018	0.036
33.7	10.332	0.172	10.413	6.086	6.315	-0.038	0.032
33.6	11.012	0.177	10.579	6.083	6.309	0.041	0.036
33.5	11.227	0.199	10.748	6.080	6.303	0.045	0.029
33.1	11.205	0.178	11.454	6.068	6.277	-0.022	0.030
33.0	11.360	0.177	11.638	6.066	6.271	-0.024	0.031
32.9	12.070	0.184	11.825	6.063	6.264	0.021	0.032
32.8	12.084	0.184	12.015	6.060	6.258	0.006	0.026
32.6	12.810	0.189	12.406	6.054	6.245	0.033	0.023

Table 3.5 (cont'd)

ALT KM	RHO-MEAS G/M**3	UNCER G/M**3	RHO-CALC G/M**3	HBAR(Z) KM	H(Z) KM	DIFF FRAC	RMS FRAC
32.4	13.332	0.192	12.818	6.048	6.233	0.041	0.027
32.2	13.400	0.192	13.228	6.042	6.221	0.013	0.026
32.1	13.876	0.195	13.443	6.039	6.214	0.032	0.028
32.0	13.995	0.219	13.661	6.037	6.208	0.024	0.030
31.6	14.413	0.195	14.572	6.025	6.184	-0.011	0.027
31.5	15.439	0.206	14.810	6.022	6.178	0.043	0.027
31.3	14.947	0.199	15.297	6.017	6.165	-0.023	0.029
31.2	15.153	0.203	15.548	6.014	6.159	-0.025	0.027
31.0	15.627	0.208	16.061	6.008	6.147	-0.027	0.028
30.8	16.701	0.221	16.593	6.002	6.135	0.007	0.027
30.7	16.723	0.221	16.866	6.000	6.129	-0.008	0.020
30.5	17.451	0.227	17.426	5.994	6.117	0.001	0.017
30.4	17.518	0.255	17.713	5.991	6.112	-0.011	0.014
30.0	19.096	0.243	18.914	5.980	6.088	0.010	0.008
29.9	19.421	0.253	19.227	5.977	6.082	0.010	0.009
29.7	19.072	0.243	19.870	5.972	6.071	-0.040	0.020
29.6	19.144	0.245	20.200	5.969	6.065	-0.052	0.031
29.5	19.605	0.258	20.536	5.966	6.059	-0.045	0.036
29.3	20.929	0.296	21.226	5.960	6.047	-0.014	0.037
29.1	20.666	0.283	21.941	5.955	6.036	-0.058	0.045
29.0	20.896	0.294	22.307	5.952	6.030	-0.063	0.050
28.9	23.378	0.444	22.681	5.949	6.025	0.031	0.046
28.6	21.589	0.327	23.840	5.941	6.008	-0.094	0.059
28.5	23.648	0.400	24.241	5.938	6.002	-0.024	0.060
28.3	24.303	0.439	25.063	5.933	5.991	-0.030	0.055
28.2	25.138	0.437	25.485	5.930	5.985	-0.014	0.048
28.1	26.962	0.433	25.914	5.927	5.980	0.040	0.050
27.9	27.242	0.445	26.797	5.922	5.969	0.017	0.027
27.7	28.263	0.498	27.711	5.917	5.957	0.020	0.026
27.6	27.341	0.449	28.180	5.914	5.952	-0.030	0.026
27.4	30.125	0.599	29.144	5.909	5.941	0.034	0.029
27.2	32.794	0.599	30.143	5.903	5.930	0.088	0.046
27.1	30.542	0.609	30.655	5.900	5.925	-0.004	0.045
27.0	32.576	0.598	31.178	5.898	5.919	0.045	0.049
26.9	31.091	0.558	31.709	5.895	5.914	-0.019	0.047
26.7	35.629	0.632	32.801	5.890	5.903	0.086	0.059
26.6	35.194	0.620	33.361	5.887	5.898	0.055	0.051
26.5	32.020	0.588	33.932	5.884	5.892	-0.056	0.057
26.3	37.662	0.671	35.105	5.879	5.882	0.073	0.062
26.2	37.429	0.669	35.707	5.876	5.876	0.048	0.065

TOT. RMS FRAC. RHOMEAS-RHOCALC DIFF= 0.04475
TOT. RMS FRAC. RHOMEAS. UNCERTAINTY= 0.03909

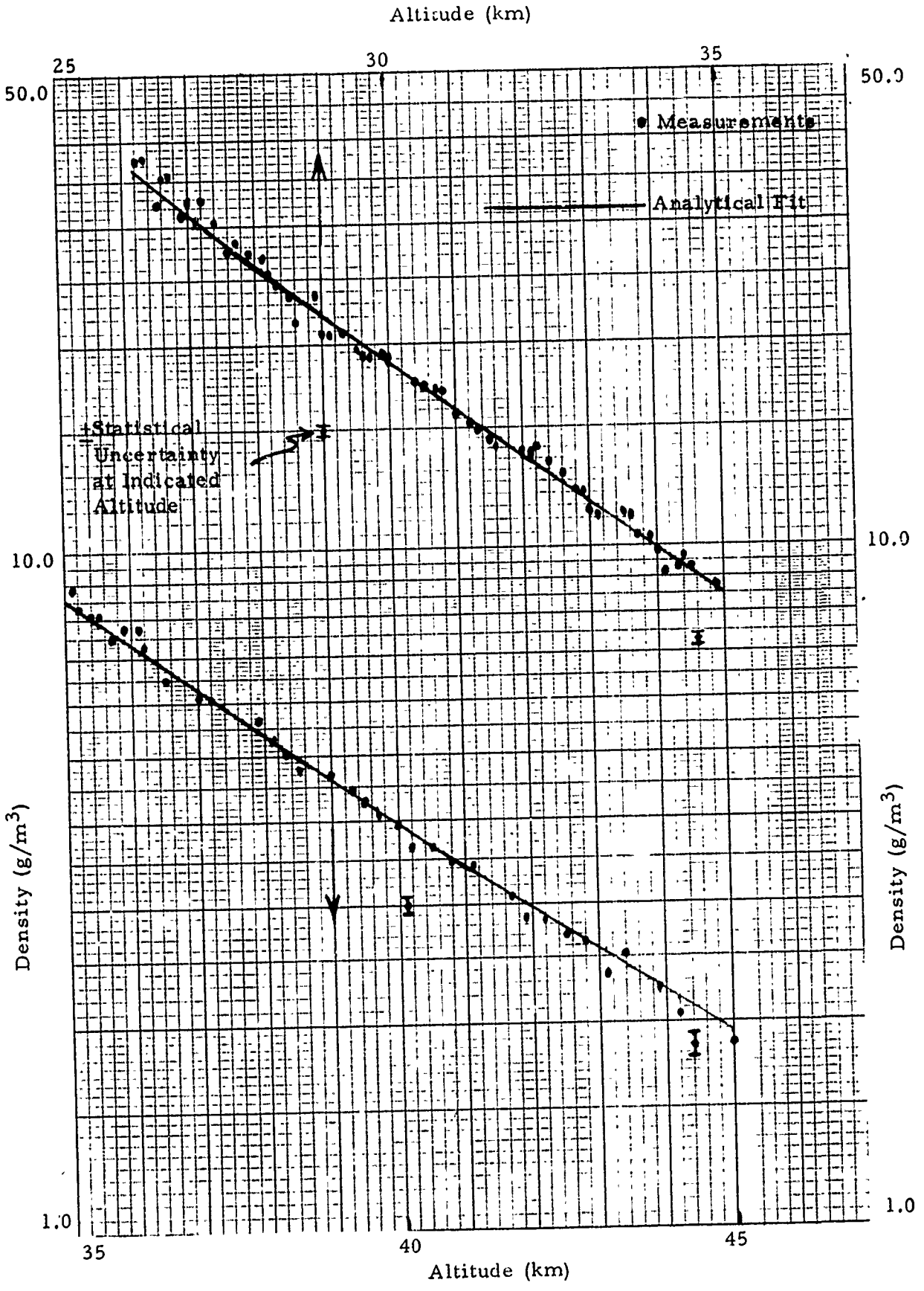

Fig. 3.1 Low Background Betasonde Air Density Results for Flight at White Sands Missile Range on 4/23/76, 25-45 km.

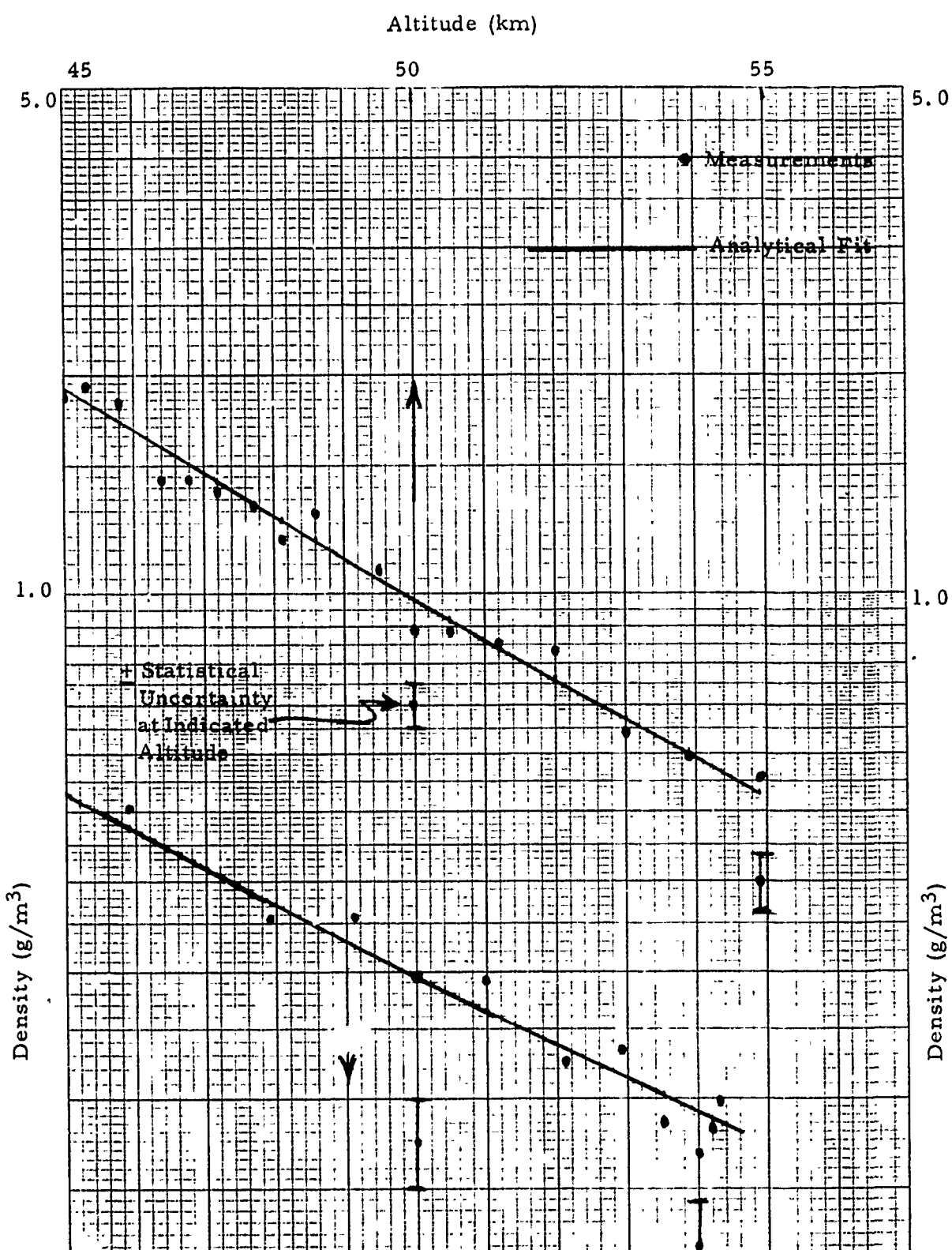

Fig. 3.2 Low Background Betasonde Air Density Results for Flight at White Sands Missile Range on 4/23/76, 45-65 km.

Examination of the variation of RMS FRAC with altitude shows those regions in which the best fit is obtained. At the highest altitudes the average difference for any single point is as high as 7-8%, due to the small number of counts recorded there. As the sonde descends it goes through a region where the average difference is on the order of 2%. There is, however, a lower altitude region (below about 20 km) in which beta particle energy loss dominates the effects of scattering, and the count rate decreases as z decreases (Ref. 3.3). Thus, near 20 km there is little variation of count rate with z, and the density uncertainty becomes very large in spite of the large count rates. This region is being approached at the lowest altitudes in Table 3.5, which accounts for much of the average difference of about 5% there. As noted previously, the 4 measurements made in the vicinity of the 64 km apogee during a period of about 20 seconds are particularly important, since the sonde descends rapidly for some distance thereafter. The data from these four points could have been averaged together to give one measurement at the average altitude of 64.0 km. The result would have been 0.1833 g/m^3 with a fractional uncertainty of .054 (about half that of each of the four points). The calculated result from the fit is .190 g/m^3, a fractional difference of only .035. Thus, these four points, as utilized with least square procedure, serve to define $\rho(z)$ accurately in the apogee altitude region.

It is of interest to compare the H(z) values with those of an appropriate model atmosphere, such as that of the Spring/Fall Mid-Latitude Model (Ref. 3.1). Values of H(z) are not given in that particular model. It is straightforward, however, to derive the associated H(z) by fitting the two $\rho(z)$ values that bracket the altitude of interest. By use of this procedure and the results of Table 3.5 we obtain the following:

Table 3.6

Comparison of Scale Heights
for 4/23/76 Flight

z(km)	H_{model}(km)	H_{fit}(km)
25	6.35	~5.85
30	6.50	6.09
35	6.47	6.40
40	6.85	6.76
45	7.24	7.18
50	8.04	7.67
55	8.40	8 24
60	8.11	8.94
65	8.08	~9.70

In general the H(z) values from the analytical fit are slightly below those of the model in the 25-30 km region, close in the 35-55 km region, and somewhat higher in the 60-65 km region. Certainly, the agreement is very reasonable on the average.

3.5 Summary and Discussion

In summary, we believe that the results of applying the least square mathematical procedure developed in Section 3.2 to the LBB flight data in Section 3.3 show the procedure to be valid. An accurate analytical fit was obtained that is capable of representing the entire tabular array of data, and we believe that the procedure should be applied to future LBB or Betasonde II flights.

It should be observed that a similar procedure can also be applied to other altitude-dependent measurements, for example temperature and pressure, provided a tabular array of the measured quantity, and its uncertainty, is available. In the case of pressure measurements the above procedure could be used almost in its exact form, since pressure also depends exponentially on altitude. For temperature the analytical function would have to be chosen to represent, in an average manner, the known variation of that quantity with altitude.

4. Atmospheric Density Response

In this section the Betasonde atmospheric density response is formulated from an analytical viewpoint, and the relative responses of various sources are derived by use of the formulation. This then allows a choice of the optimum source for the sonde, and a calculation of the expected accuracy.

4.1 Formulation

Consider the beta particle forward scattering configuration shown in Fig. 4.1.

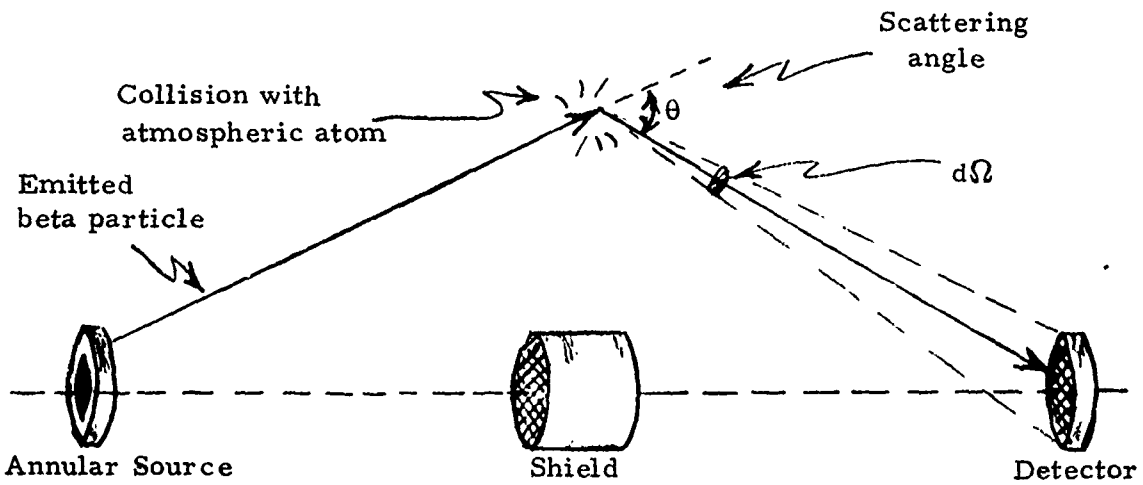

Fig. 4.1 Beta-ray Scattering Configuration

The single-scattering count rate $C_s(E_t)$ cps of the detector for the source s and detector energy threshold E_t (the energy above which all electrons are counted) is found by integrating over all scattering angles θ into solid angles dΩ:

$$C_s(E_t) = \rho\,(nN_o/M) \iint_{\Omega\ E_t}^{\infty} S_s(E_t) B_s(E) d\sigma(E,\theta) dE \qquad (4.1)$$

Here ρ = atmospheric density, g/cm^3
N_o = Avogadro's number, 6.023×10^{23} molecules/(g-mole)
M = molecular weight of atmosphere, g-mole
n = number of atmospheric atoms/molecule
$d\sigma = f(\theta)F(E)d\Omega$ cm^2/atom

$F(E) = (1-\beta^2)/\beta^4$
$f(\theta) = (Z^2 r_o^2/4)\ \mathrm{Sin}^{-4}\theta/2\ \ \mathrm{cm}^2/(\mathrm{sr\text{-}atom})$
$\beta = v/c$ = ratio of beta particle velocity to that of light
Z = atomic number of atmosphere
r_o = classical electron radius, 2.82×10^{-13} cm
$S_s(E_t)$ = total emission rate of source for particles of energy greater than E_t, β/sec
$B_s(E)$ = spectrum for beta source of type s, normalized to unity from E_t to ∞, β/keV
E = kinetic energy, keV

The cross section $d\sigma(E, \theta)$ for scattering of an electron of energy E (in the energy range of interest here, $\gtrsim 50$ keV) through an angle θ is given by Evans (Ref. 4.1). As shown above, it is separable into two functions, the first depending only on E, and the second only on θ. The function F(E) can be written conveniently in terms of the energy E as

$$F(E) = \left[\frac{1+R}{(1+R)^2 - 1}\right]^2, \tag{4.2}$$

where
$$R = E/(m_o c^2) \tag{4.3}$$

and
$$m_o c^2 = 511 \text{ keV} \tag{4.4}$$

is the electron's rest mass energy.

Because the energy and angular integrations can be separated, we write the count rate in terms of the single scattering constant K_s,

$$C_s(E_t) = K_s(E_t)\rho \text{ cps}, \tag{4.5}$$

where
$$K_s(E_t) = GS_s(E_t)\,\xi_s(E_t)\ (\mathrm{cps\text{-}cm}^3)/\mathrm{g}, \tag{4.6}$$

G is a constant for a given geometry and gas,

$$G = (nN_o/M)\int_{\Omega} f(\theta)d\Omega\ \frac{\mathrm{cm}^3}{\mathrm{g}\text{-}\beta}, \tag{4.7}$$

and the "beta source efficiency factor" is

$$\xi_s(E_t) = \int_{E_t}^{\infty} B_s(E)F(E)dE. \tag{4.8}$$

For any particular beta source, the spectrum $B_s(E)$ is either known or can be measured. Hence the efficiency factor $\mathcal{E}_s(E_t)$ can be readily determined for any threshold energy E_t. Suppose for that particular source the constant $K_s(E_t)$ has been determined by measuring the slope of the count rate versus density curve for the gas of interest. Then the constant G for that geometry and gas can be calculated from

$$G = K_s(E_t)/[S_s(E_t)\,\mathcal{E}_s(E_t)] \tag{4.9}$$

As a consequence, for any other source the value of $K_s(E_t)$ can be determined for that gas and any desired energy threshold from (4.6).

4.2 Beta Source Evaluation

From (4.5) it is clear that the larger is $K_s(E_t)$ the higher will be the count rate for any density ρ. $K_s(E_t)$ depends on E_t through both the efficiency factor and the emission rate $S_s(E_t)$ of betas having energy greater than E_t. It is convenient to write this as

$$S_s(E_t) = f_s(E_t)S_{so} \tag{4.10}$$

where S_{so} is the total emission rate (β/sec) and $f_s(E_t)$ is the fraction of those betas that have energy greater than E_t for the source type s.

In the present instrument the energy threshold E_t must be set at about 50 keV in order to exceed the electronic noise sufficiently. This means that a beta source such as Ni-63, with a maximum energy of 67 keV, will not have a large value of $f(E_t)$. However, the fact that the maximum energy is only 67 keV causes $\mathcal{E}(E_t)$ to be large. Thus we rewrite $K_s(E_t)$ as follows:

$$K_s(E_t) = GS_{so}Q_s(E_t) \tag{4.11}$$

where

$$Q_s(E_t) = f_s(E_t)\,\mathcal{E}_s(E_t) \tag{4.12}$$

measures the overall "quality" of the source of type s for the energy threshold E_t. Thus

$$Q_s(E_t) = C(E_t)/(G\rho\,S_{so}) \tag{4.13}$$

determines the count rate per unit of total source activity and per unit density for a fixed energy threshold E_t and geometry.

Table 4.1a
BETA SOURCE TYPE IS TL204

I	E KEV	BS(E) 1/KEV	F(E)	EP(E) 1/KEV
1	55.0	0.002392	23.8406	0.0570258
2	65.0	0.002369	17.3541	0.0411091
3	75.0	0.002346	13.2465	0.0310728
4	85.0	0.002334	10.4761	0.0244532
5	95.0	0.002311	8.5160	0.0196810
6	105.0	0.002288	7.0758	0.0161892
7	115.0	0.002265	5.9851	0.0135554
8	125.0	0.002242	5.1382	0.0115185
9	135.0	0.002219	4.4666	0.0099096
10	145.0	0.002207	3.9244	0.0086614
11	155.0	0.002196	3.4800	0.0076405
12	165.0	0.002172	3.1108	0.0067578
13	175.0	0.002161	2.8004	0.0060513
14	185.0	0.002149	2.5369	0.0054525
15	195.0	0.002138	2.3110	0.0049403
16	205.0	0.002126	2.1158	0.0044985
17	215.0	0.002115	1.9458	0.0041147
18	225.0	0.002103	1.7968	0.0037788
19	235.0	0.002092	1.6654	0.0034832
20	245.0	0.002068	1.5488	0.0032036
21	255.0	0.002045	1.4449	0.0029552
22	265.0	0.002011	1.3518	0.0027180
23	275.0	0.001988	1.2681	0.0025203
24	285.0	0.001964	1.1924	0.0023424
25	295.0	0.001941	1.1238	0.0021817
26	305.0	0.001907	1.0614	0.0020237
27	315.0	0.001884	1.0044	0.0018919
28	325.0	0.001860	0.9523	0.0017716
29	335.0	0.001837	0.9043	0.0016616
30	345.0	0.001814	0.8602	0.0015606
31	355.0	0.001780	0.8195	0.0014583
32	365.0	0.001745	0.7818	0.0013642
33	375.0	0.001710	0.7469	0.0012773
34	385.0	0.001687	0.7144	0.0012053
35	395.0	0.001652	0.6842	0.0011305
36	405.0	0.001618	0.6560	0.0010612
37	415.0	0.001583	0.6296	0.0009967
38	425.0	0.001537	0.6049	0.0009296
39	435.0	0.001491	0.5817	0.0008672
40	445.0	0.001456	0.5600	0.0008153
41	455.0	0.001421	0.5395	0.0007668
42	465.0	0.001375	0.5203	0.0007154
43	475.0	0.001329	0.5021	0.0006672
44	485.0	0.001271	0.4849	0.0006163
45	495.0	0.001213	0.4687	0.0005686
46	505.0	0.001167	0.4533	0.0005290
47	515.0	0.001121	0.4387	0.0004917
48	525.0	0.001075	0.4249	0.0004566
49	535.0	0.001017	0.4117	0.0004187
50	545.0	0.000959	0.3992	0.0003829
51	555.0	0.000901	0.3874	0.0003491
52	565.0	0.000855	0.3760	0.0003215
53	575.0	0.000797	0.3652	0.0002912
54	585.0	0.000740	0.3549	0.0002625
55	595.0	0.000682	0.3451	0.0002353
56	605.0	0.000624	0.3356	0.0002094
57	615.0	0.000566	0.3266	0.0001849
58	625.0	0.000520	0.3180	0.0001654
59	635.0	0.000474	0.3098	0.0001468
60	645.0	0.000416	0.3018	0.0001256
61	655.0	0.000358	0.2942	0.0001054
62	665.0	0.000300	0.2869	0.0000862
63	675.0	0.000254	0.2799	0.0000712
64	685.0	0.000208	0.2732	0.0000568
65	695.0	0.000173	0.2667	0.0000462
66	705.0	0.000139	0.2605	0.0000361
67	715.0	0.000104	0.2545	0.0000265
68	725.0	0.000069	0.2487	0.0000172
69	735.0	0.000046	0.2431	0.0000112
70	745.0	0.000023	0.2377	0.0000055
71	755.0	0.000000	0.2325	0.0000000

DENSITY EFFICIENCY FACTOR= 3.24197

Table 4.1 Tabulation of Calculation for Density Efficiency Factors

a) Thallium 204
b) Strontium-Yttrium 90
c) Nickel 63
d) Promethium 147

By use of a tabulation of beta spectra (Ref. 4.2) for Tl-204, Sr-Y-90, and Ni-63, and an experimental measurement for Pm-147, the results given in Table 4.1 were obtained for E_t = 50 keV. This is a tabulation of $B_s(E)$, $F(E)$, and $\xi(E) = B_s(E)F(E)$ versus energy for each of these sources. At the end of each tabulation is the result obtained for $\xi_s(E_t)$ from (4.8). By use of these results, and the fractions $f_s(E_t)$ found from Ref. 4.2, we then obtain the results in Table 4.2.

Table 4.1b

BETA SOURCE TYPE IS SRY90

I	E KEV	BS(E) 1/KEV	F(E)	EP(E) 1/KEV
1	62.5	0.001609	18.6935	0.0300791
2	87.5	0.001620	9.9243	0.0160761
3	112.5	0.001631	6.2316	0.0101617
4	137.5	0.001641	4.3203	0.0070917
5	162.5	0.001647	3.1970	0.0052650
6	187.5	0.001631	2.4772	0.0040395
7	212.5	0.001609	1.9862	0.0031959
8	237.5	0.001587	1.6349	0.0025954
9	262.5	0.001544	1.3742	0.0021221
10	287.5	0.001469	1.1746	0.0017252
11	312.5	0.001393	1.0182	0.0014184
12	337.5	0.001290	0.8930	0.0011524
13	362.5	0.001188	0.7910	0.0009396
14	387.5	0.001031	0.7067	0.0007288
15	412.5	0.000875	0.6360	0.0005563
16	437.5	0.000718	0.5762	0.0004138
17	462.5	0.000594	0.5250	0.0003118
18	487.5	0.000481	0.4808	0.0002310
19	512.5	0.000373	0.4423	0.0001648
20	537.5	0.000324	0.4086	0.0001324
21	562.5	0.000335	0.3788	0.0001268
22	587.5	0.000340	0.3524	0.0001199
23	612.5	0.000346	0.3289	0.0001136
24	637.5	0.000346	0.3077	0.0001063
25	662.5	0.000351	0.2887	0.0001013
26	687.5	0.000351	0.2715	0.0000953
27	712.5	0.000351	0.2559	0.0000898
28	737.5	0.000356	0.2417	0.0000861
29	762.5	0.000356	0.2287	0.0000815
30	787.5	0.000356	0.2168	0.0000773
31	812.5	0.000356	0.2059	0.0000734
32	837.5	0.000356	0.1958	0.0000698
33	862.5	0.000351	0.1865	0.0000654
34	887.5	0.000351	0.1778	0.0000624
35	912.5	0.000351	0.1698	0.0000596
36	937.5	0.000351	0.1623	0.0000570
37	962.5	0.000351	0.1554	0.0000545
38	987.5	0.000346	0.1489	0.0000515
39	1012.5	0.000346	0.1428	0.0000494
40	1037.5	0.000346	0.1371	0.0000474
41	1062.5	0.000346	0.1318	0.0000455
42	1087.5	0.000340	0.1268	0.0000431
43	1112.5	0.000340	0.1221	0.0000415
44	1137.5	0.000335	0.1176	0.0000394
45	1162.5	0.000329	0.1134	0.0000374
46	1187.5	0.000329	0.1094	0.0000360
47	1212.5	0.000324	0.1057	0.0000342
48	1237.5	0.000319	0.1021	0.0000325
49	1262.5	0.000313	0.0987	0.0000309
50	1287.5	0.000313	0.0955	0.0000299
51	1312.5	0.000308	0.0925	0.0000285
52	1337.5	0.000297	0.0896	0.0000266
53	1362.5	0.000286	0.0868	0.0000248
54	1387.5	0.000281	0.0842	0.0000236
55	1412.5	0.000275	0.0817	0.0000225
56	1437.5	0.000270	0.0793	0.0000214
57	1462.5	0.000265	0.0770	0.0000204
58	1487.5	0.000254	0.0748	0.0000190
59	1512.5	0.000248	0.0728	0.0000181
60	1537.5	0.000238	0.0708	0.0000168
61	1562.5	0.000232	0.0688	0.0000160
62	1587.5	0.000221	0.0670	0.0000148
63	1612.5	0.000216	0.0652	0.0000141
64	1637.5	0.000205	0.0636	0.0000130
65	1662.5	0.000194	0.0619	0.0000120
66	1687.5	0.000184	0.0604	0.0000111
67	1712.5	0.000173	0.0589	0.0000102
68	1737.5	0.000162	0.0574	0.0000093
69	1762.5	0.000151	0.0560	0.0000085
70	1787.5	0.000140	0.0547	0.0000077
71	1812.5	0.000130	0.0534	0.0000069
72	1837.5	0.000119	0.0522	0.0000062
73	1862.5	0.000108	0.0510	0.0000055
74	1887.5	0.000097	0.0498	0.0000048
75	1912.5	0.000086	0.0487	0.0000042
76	1937.5	0.000076	0.0476	0.0000036
77	1962.5	0.000065	0.0466	0.0000030
78	1987.5	0.000054	0.0456	0.0000025
79	2012.5	0.000043	0.0446	0.0000019
80	2037.5	0.000032	0.0436	0.0000014

Table 4.1b, cont'd (SRY90)

I	E KEV	BS(E) 1/KEV	F(E)	EF(E) 1/KEV
81	2062.5	0.000022	0.0427	0.0000009
82	2087.5	0.000016	0.0418	0.0000007
83	2112.5	0.000011	0.0410	0.0000004
84	2137.5	0.000005	0.0402	0.0000002
85	2162.5	0.000000	0.0394	0.0000000

DENSITY EFFICIENCY FACTOR= 2.26852

Table 4.1c

BETA SOURCE TYPE IS NI63

I	E KEV	BS(E) 1/KEV	F(E)	EF(E) 1/KEV
1	50.5	0.170520	28.0649	4.7856388
2	51.5	0.141619	27.0314	3.8281451
3	52.5	0.119942	26.0554	3.1251457
4	53.5	0.101156	25.1328	2.5423382
5	54.5	0.086705	24.2597	2.1034450
6	55.5	0.073699	23.4326	1.7269720
7	56.5	0.062139	22.6483	1.4073390
8	57.5	0.052023	21.9039	1.1395103
9	58.5	0.043353	21.1967	0.9189316
10	59.5	0.037572	20.5242	0.7711404
11	60.5	0.031792	19.8842	0.6321561
12	61.5	0.026012	19.2746	0.5013618
13	62.5	0.020231	18.6935	0.3781912
14	63.5	0.014451	18.1391	0.2621252
15	64.5	0.010116	17.6098	0.1781335
16	65.5	0.005780	17.1041	0.0988674
17	66.5	0.002890	16.6206	0.0480363

DENSITY EFFICIENCY FACTOR=24.44748

Table 4.1d

BETA SOURCE TYPE IS PM147

I	E KEV	BS(E) 1/KEV	F(E)	EF(E) 1/KEV
1	52.5	0.016595	26.0554	0.4323827
2	57.5	0.015827	21.9039	0.3466808
3	62.5	0.015060	18.6935	0.2815225
4	67.5	0.014197	16.1580	0.2293888
5	72.5	0.013621	14.1194	0.1923217
6	77.5	0.012854	12.4549	0.1600920
7	82.5	0.011990	11.0776	0.1328244
8	87.5	0.011223	9.9243	0.1113805
9	92.5	0.010456	8.9486	0.0935628
10	97.5	0.009784	8.1153	0.0794017
11	102.5	0.009017	7.3978	0.0667047
12	107.5	0.008058	6.7754	0.0545928
13	112.5	0.007194	6.2316	0.0448318
14	117.5	0.006427	5.7537	0.0369783
15	122.5	0.005659	5.3313	0.0301722
16	127.5	0.004988	4.9559	0.0247202
17	132.5	0.004412	4.6208	0.0203892
18	137.5	0.003837	4.3203	0.0165767
19	142.5	0.003357	4.0497	0.0135962
20	147.5	0.002878	3.8051	0.0109500
21	152.5	0.002494	3.5833	0.0089367
22	157.5	0.002110	3.3813	0.0071357
23	162.5	0.001727	3.1970	0.0055200
24	167.5	0.001439	3.0282	0.0043571
25	172.5	0.001247	2.8732	0.0035829
26	177.5	0.000959	2.7306	0.0026192
27	182.5	0.000767	2.5989	0.0019944
28	187.5	0.000576	2.4772	0.0014257
29	192.5	0.000384	2.3644	0.0009077
30	197.5	0.000288	2.2596	0.0006502
31	202.5	0.000192	2.1620	0.0004148
32	207.5	0.000192	2.0711	0.0003973
33	212.5	0.000096	1.9862	0.0001905
34	217.5	0.000096	1.9067	0.0001829
35	222.5	0.000000	1.8323	0.0000000

DENSITY EFFICIENCY FACTOR=12.08692

Table 4.2

Atmospheric Density Measurement
Evaluation Factors, E_t = 50 keV

Source Type	Half-life (yrs)	$f_s(E_t)$	$\mathcal{E}_s(E_t)$	$Q_s(E_t)$
Thallium-204	3.6	.14	3.24	.45
Strontium-Yttrium-90	28	.95	2.27	2.16
Nickel-63	120	.02	24.45	.49
Promethium-147	2.5	.50	12.09	6.05

The higher is the value of Q_s the smaller is the amount of source activity required to obtain the same count rate (i. e., density accuracy) at a given density. From that viewpoint, Pm-147 is the best choice. Unfortunately, it has the shortest half-life and would probably require calibration of a given sonde at least on an annual basis. It is, however, available at a reasonable price (less than about $1000) in higher activity amounts (up to about a curie in the annular configuration used here) than any of the others. If it were possible to develop a detector with a much lower energy threshold ($\lesssim$10-20 keV), then the Ni-63 source would definitely be optimum. In that case $f_s(E_t)$ would be near 0.50, and $\mathcal{E}_s(E_t)$ would be even larger. This would be necessary, because the source is not readily available in amounts larger than 50-100 mCi.

For the present system we believe that Pm-147 is optimum. It will provide a means of establishing the utility of the betasonde for the upper portion of the middle atmosphere.

4.3 Estimated Density Accuracy

The source strength of the same annular Pm-147 beta source previously flown on the Low Background Betasonde (LBB) has been measured on May 12, 1977 to be

$$S_s(E_t) = 2.76 \times 10^9 \ \beta/\text{sec} = 74.5 \ \text{mCi} \quad \text{(test source)} \tag{4.14}$$

for E_t = 50 keV. The slope of the count rate versus density, Eq. (4.5), was measured in the geometry of Fig. 2.1 to obtain the calibration constant

$$K_s(E_t) = 0.93 \times 10^9 \ \text{cps}/(\text{g/cm}^3) \quad \text{(test source)} \tag{4.15}$$

for the source intensity (4.14).

A difference between the present sonde and the LBB is that a significant wall effect is present during calibration in the Panametrics chamber (about 2'x3'). This was not experienced by the LBB due, we believe, to the extremely collimated geometry of the geiger counters themselves. Thus, going to the semiconductor detectors causes a significant increase in overall efficiency, but also produces a wall effect in the small chamber. This does not affect the determination of the constant K_s, since it is the slope of the count rate versus density curve. It does mean, however, that in order to obtain an actual calibration curve at densities less than that equivalent to about 70 km, it will be necessary to use a much larger chamber. Such chambers are available at NASA Langley Research Center (both 20' and 60' diameter spheres) and have been used previously (Ref. 3.3) for betasonde calibration work.

Once it is established that a calibration measurement K_s in a small chamber leads to the same result as that obtained in a large chamber - in which the wall effect is much reduced - it is not then necessary to recalibrate in the large chamber unless the source-detector geometry is changed in some significant way. Rather, a value of K_s can be carefully measured in the small chamber in the $z \leq 60$ km region, where the wall effect is only a fraction of total count rate, even in the small chamber, and the calibration curve for higher altitudes can be obtained by extrapolation. This is possible because single-scattering is by far the dominant effect for $z \gtrsim 40$ km, hence the calibration curve is extremely linear and the count rate versus density is given rigorously by Eq. (4.5).

Thus, the calibration results in the small chamber can be used to estimate the accuracy obtainable at high altitudes and with a more intense source.

The fractional statistical uncertainty for any count rate C_s measured for a time t(sec) is given by (Ref. 3.2)

$$\Delta\rho/\rho = 1/\sqrt{Ct} \tag{4.16}$$

By use of (4.5) this is

$$\Delta\rho/\rho = 1/\sqrt{K_s(E_t)\rho t} \tag{4.17}$$

This shows explicity that the statistical uncertainty is a function of the threshold E_t through the calibration constant $K_s(E_t)$. Of course, K_s is also proportional to the source strength $S_s(E_t)$ through (4.6). We believe that a source of intensity about 5 times higher than (4.14) should be obtained to use as the first flight source,

$$S_s(E_t) = 1.38 \times 10^{10}\ \beta/\text{sec} = 373\ \text{mCi}, \quad \text{(flight source)} \tag{4.18}$$

for which

$$K_s(E_t) = 4.65 \times 10^{9}\ \text{cps}/(\text{g/cm}^3). \quad \text{(flight source)} \tag{4.19}$$

Now, by use of the standard atmosphere densities (Ref. 4.3), Eqs. (4.5), (4.19) and (4.17), the following results are obtained:

Table 4.3

Estimated Fractional Statistical Uncertainty for Betasonde II and First Flight Source ($S_s \approx 373$ mCi)

Z km	ρ g/cm^3	C_s cps	$\Delta\rho/\rho$ t = 20 sec	t = 5 sec	t = 1 sec
60	3.1×10^{-7}	1441	.006	.012	.026
70	8.8×10^{-8}	409.2	.011	.022	.049
80	2.0×10^{-8}	93.0	.023	.046	.104
90	3.2×10^{-9}	14.9	.058	.116	.259
100	5.0×10^{-10}	2.3	.147	.295	.659

The uncertainties listed in this table are, of course, the minimum that will occur for the indicated count rates. The actual total error will be slightly larger due to some (as yet undetermined) cosmic ray effect. This is expected to be extremely small, however; much less than in the LBB (Ref. 3.2).

As seen from Table 3.1, the betasonde spends about 20 seconds within a 1 km region near apogee. As discussed above, this allows a very accurate measurement of the density in this particular region; the procedure described in Section 3 provides an analytical density fit that takes this into account. The RMS deviation of the fit from the measured results approaches the statistical accuracy both in that high altitude region and on an overall average basis (Table 3.5). Thus, it can be expected that the accuracy of the fit would approach about $\pm$6% near 90 km for an apogee in that region. At lower altitudes, as the descent velocity increases, it was found that 5 second intervals provided a meaningful measurement. Hence from about 80 km downward to perhaps 40-50 km the accuracy will be no worse than about $\pm$5%, as seen in Table 4.3.

5. Phase I Summary

During Phase I, Research and Development, the following work has been accomplished.

1. A technique has been developed for making an analytic fit to an entire array of density versus altitude data on a least-square-basis. The procedure was applied to data from a Low Background Betasonde flight with good results.
2. By use of theoretical calculations and experimental measurements, it was shown that Pm-147 is the optimum choice source for the single-scattering betasonde. This conclusion would be modified if it were possible to reduce the energy threshold (that energy above which all betas are counted), to about 10-20 keV. In that case Ni-63 would probably be optimum.
3. A laboratory model of Betasonde II, the semiconductor-detector version, has been constructed and calibrated with Pm-147. Although some wall-effect count rate was evident at very low densities (due, apparently, to the open geometry of the detector), it was possible to obtain meaningful calibration data.
4. The calibration data were used to show that with a Pm-147 source of about 500 mCi, it should be possible to obtain about $\pm 6\%$ accuracy in the 90 km region for an Arcas launch having apogee near that altitude. Below that altitude the accuracy would be better.
5. The flight instrument must, ultimately, be calibrated in a large (40'x60') chamber in order to verify the high altitude ($\gtrsim$70 km) portion of the calibration curve.

During Phase II, Design and Fabrication, the flight unit will be completed and tested. It will be calibrated by use of the new ~500 mCi Pm-147 source, and the unit will be ready for delivery at the completion of the work. During the final phase of the work (not presently expected to be funded by the Army Research Office) the instrument must be integrated into an Arcas payload for launch at White Sands Missile Range. The Betasonde II should then be flown to the 80-90 km region at least twice, and the analytical fitting procedure presented above should be applied to the data. This will form the basis for routine direct measurement of atmospheric density up to at least the 80-90 km region. Should this prove to be feasible, as is expected based on the present results, it would then be useful to consider application of the technique up to the 100 km region either by use of a more intense source (several kCi), by developing detection techniques allowing a lower energy threshold ($\lesssim$10-20 keV), or a combination of these measures.

References

3.1 U.S. Standard Atmosphere Supplements, 1966, U.S. Government Printing Office, Washington, D.C. 20402 (1966).

3.2 B. Sellers, F. A. Hanser, and J. L. Hunerwadel, Stratcom VI-A UV Flux and 30-65 km Low-Background Betasonde Air Density Measurements, PANA-AIR-1 (July, 1976).

3.3 B. Sellers, H. N. Ballard and M. Izquierdo, Direct Measurement of Air Density in the 30-60 km Region by Beta-Ray Forward Scattering, J. Appl. Rad. Iso. 20, 341-351 (1969).

4.1 R. D. Evans, The Atomic Nucleus, McGraw-Hill, N.Y. (1955).

4.2 O. H. Hogan, P. E. Zigman, and J. L. Mackin, Beta Spectra II. Spectra of Individual Negatron Emitters, USNRDL-TR-802 (Dec. 1964). AD455961.

4.3 U. S. Standard Atmosphere 1962. U.S. Government Printing Office, Washington, D.C. 20402 (1962). AD401813.